S43A-2469, AGU 2013

Period Dependence on Source Process of the 2011 Tohoku Earthquake by Multi Period-band Waveform Inversions

Hisahiko Kubo[1], Kimiyuki Asano[1], Tomotaka Iwata[1], Shin Aoi[2]
[1] DPRI, Kyoto Univ., Uji, Japan, [2] NIED, Tsukuba, Japan
E-mail: kubo.hisahiko.26a@st.kyoto-u.ac.jp

Abstract

Based on the comparison among source models having different analysis period-band (10-25s, 25-50s, and 50-100s), we constructed the broadband source model for the 2011 Tohoku earthquake on the period band of 10-100s. This constructed model consists of four main rupture: a shallow rupture off Miyagi at 45-90s toward up-dip having long duration, twice deep ruptures off Miyagi toward down-dip at 0-60s and 45-90s, and a deep rupture off Fukushima at 90-150s. The seismic-wave radiation from the second deep rupture off Miyagi has richer long-period component than that from the first one, and this may be due to the effect of the twice fault rupture.

Introduction

From the comparison between slip model using long-period (10s~) seismic waves and excitation zones of short-period (0.1-10s) seismic waves, it has been suggested that the 2011 Tohoku earthquake (Mw9.0) has the period-dependent spatial variation on the seismic-wave radiation and this variation would be caused by the spatial difference of slip behavior on the plate boundary (e.g., Koper et al., 2011; Ide et al., 2011). However, their studies were based on the qualitative comparison of the results obtained by different methods, and the quantitative comparison between source models having different period-bands has not been made. Therefore, the construction of the source models at different period-bands by a common method is important for further understandings of the source characteristics of the 2011 Tohoku earthquake. In this study, we construct the spatiotemporal slip models for the 2011 Tohoku earthquake on three different period bands (10-25s, 25-50s, and 50-100s) using teleseismic and strong-motion data, and discuss the source characteristics of this earthquake based on the spatial differences of estimated slip-velocity time function in different period-bands.

■ Period-dependent seismic-wave radiation

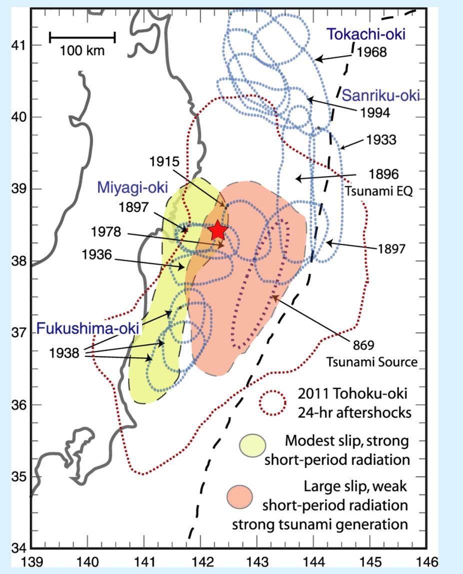

* After Kopper et al. (2011)

■ Flow chart of this study

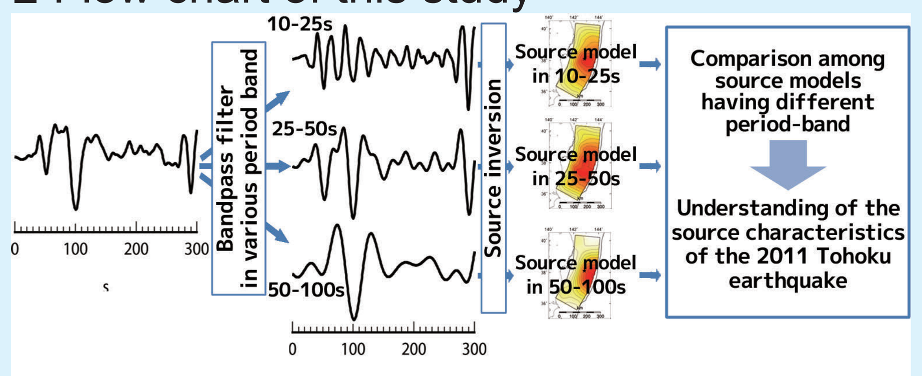

Data & Method

■ Teleseismic station map

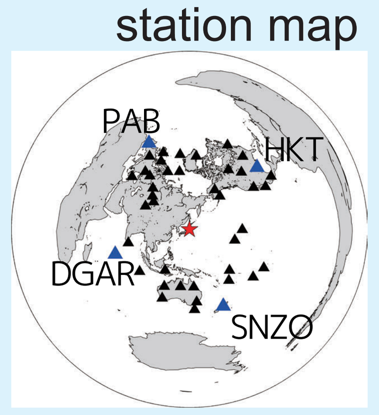

■ Strong-motion station map

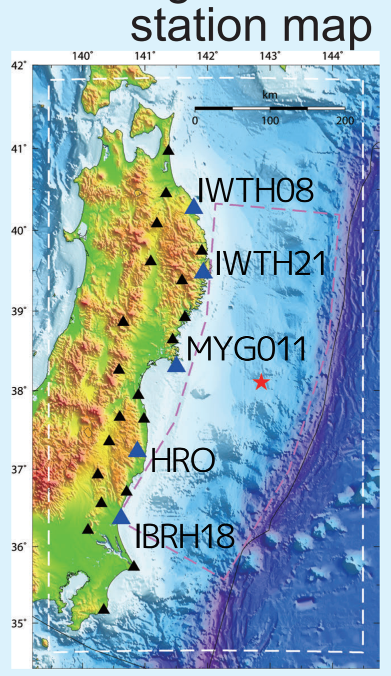

* White line: Calculation area in GMS

The teleseismic data is the vertical-component displacement waveforms at 42 IRIS stations (Time length is 300s starting 10s before the P-wave arrival). The strong-motion data is three components of velocity waveforms at 25 stations of K-NET, KiK-net, and F-net (Time length is 150-300s starting 10s before the P-wave arrival).

The teleseicmic Green's functions are the same as those used in Kubo & Kakehi (2013). The strong-motion Green's functions are calculated by the 3D FDM (GMS; Aoi & Fujiwara, 1999) using a 3D velocity structure model, Japan Integrated Velocity Structure Model Version 1 (Koketsu et al., 2012).

The spatiotemporal rupture history is estimated by the kinematic linear waveform inversion using multiple time windows (Hartzell & Heaton, 1983) with the spatiotemporal smoothing constraint on slips proposed by Kubo & Kakehi (2013). The slip time history of each subfault is represented by the superposition of 24 smoothed ramp functions with 8.0s width, each of which is put with 4.0s lag. The maximum slip duration at each subfault and the propagation velocity of the first time window are set to 100s and 2 km/s, respectively, with reference to Kubo & Kakehi (2013). The assumed fault geometry is the same as that used in Kubo & Kakehi (2013).

Comparison among Source Models Having Different Analysis Period-band

Teleseismic Model

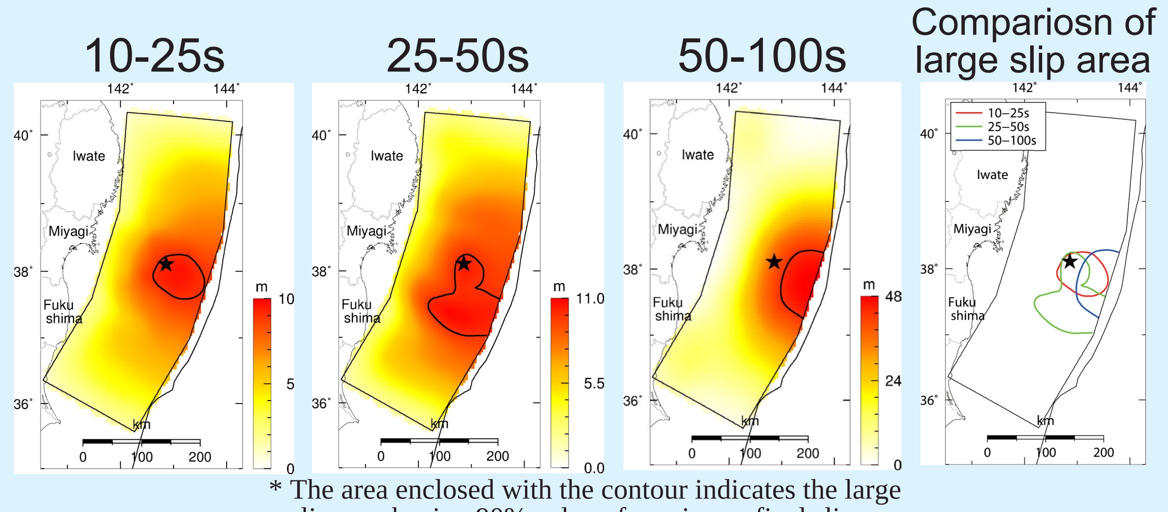

* The area enclosed with the contour indicates the large slip area having 90% value of maximum final slip.

Strong-Motion Model

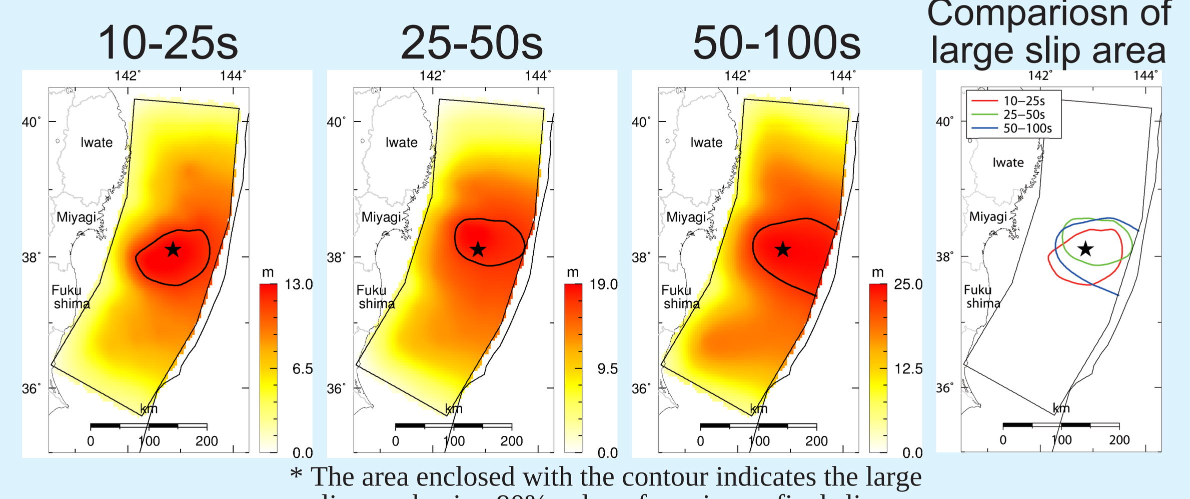

* The area enclosed with the contour indicates the large slip area having 90% value of maximum final slip.

■ Final slip distributions

・Estimated model parameters

	Teleseismic			Strong-Motion		
	10-25s	25-50s	50-100s	10-25s	25-50s	50-100s
Mo ($*10^{22}$Nm)	1.7	2.2	5.4	2.5	3.7	5.5
Mw	8.8	8.8	9.1	8.9	9.0	9.1
Max. Slip (m)	10	11	48	13	19	25

・Location of large slip area having 90% value of maximum final slip

10-25s & 25-50s models	Slightly shallow part
50-100s model	Shallowest part

■ Temporal slip progressions (15 s time step)

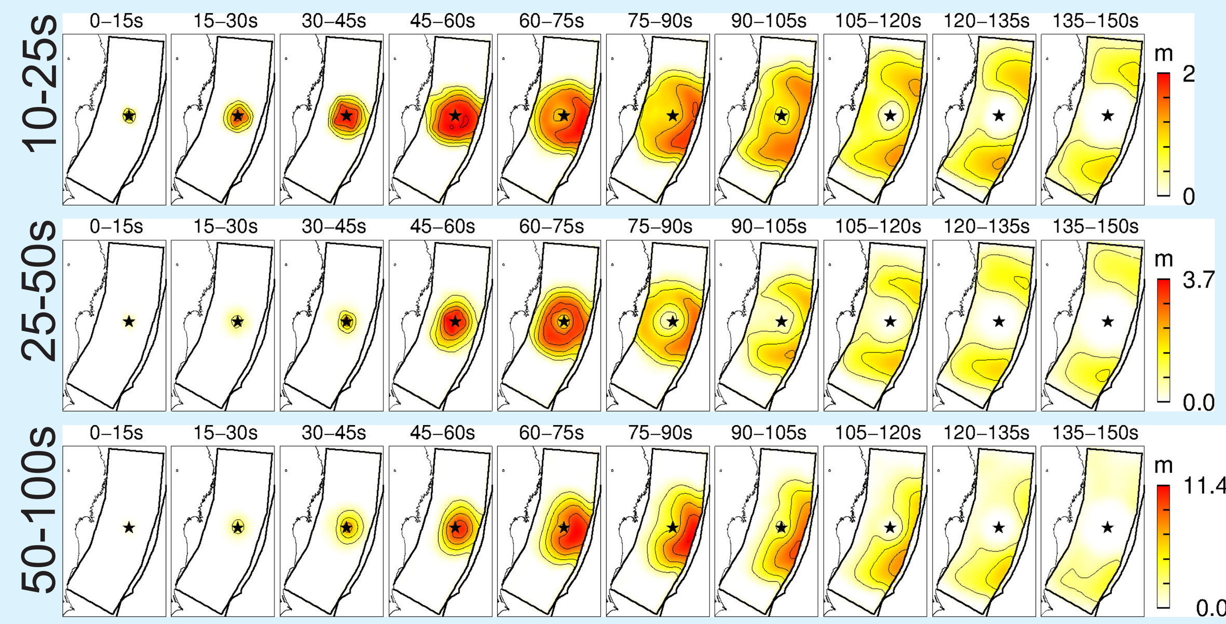

○Region off Miyagi

・10-25s & 25-50s models: Shallow rupture toward up-dip + Twice deep ruptures toward down-dip

・50-100s model: Distinct Shallow rupture toward up-dip + Deep rupture toward down-dip

○Region off Fukushima: Deep rupture at 90-150s

○These deep ruptures are consistent with SMGA model.

* In this study, "Shallow (Deep) rupture" is explaining the rupture on the shallower (deeper) plate-boundary area than the focal depth.

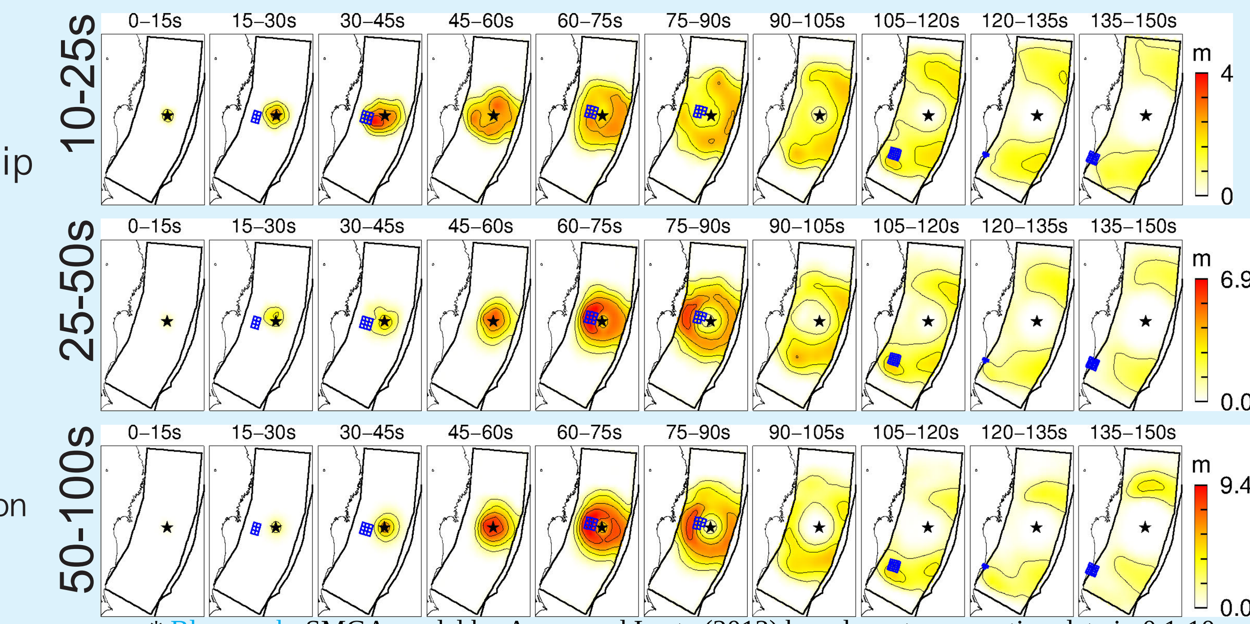

* Blue mesh: SMGA model by Asano and Iwata (2012) based on strong-motion data in 0.1-10 s.

■ Slip-velocity time functions

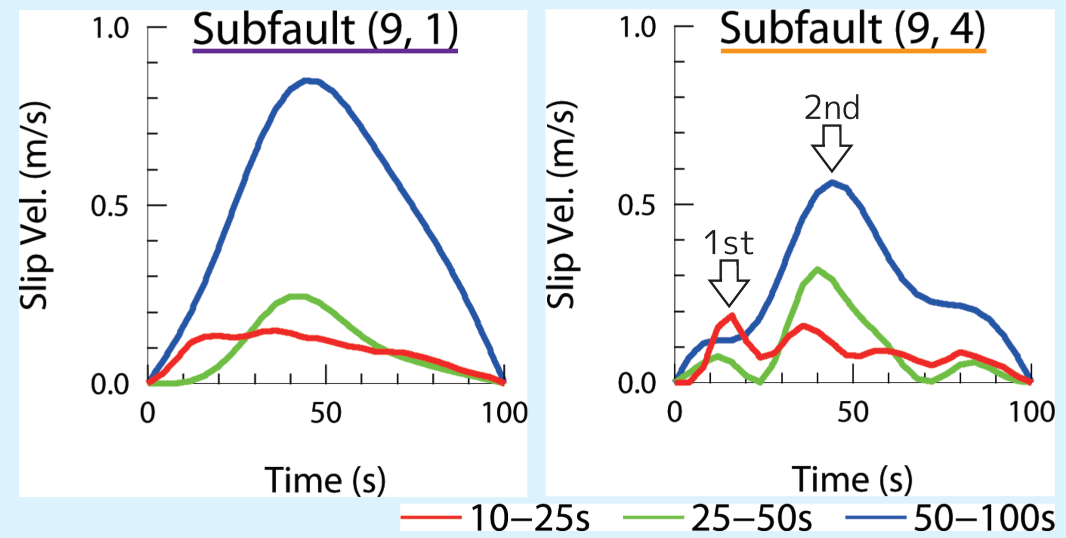

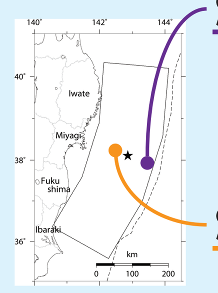

Subfault (9,1) (Shallowest)

・Simple shape having long duration.

・The shape of 10-25s model leans forward compared to others.

Subfault (9,4) (Slightly deep)

・Distinct two peaks → Twice rupture

・Max. timing of 10-25s model: 1st peak
Max. timing of 25-50s & 50-100s models: 2nd peak

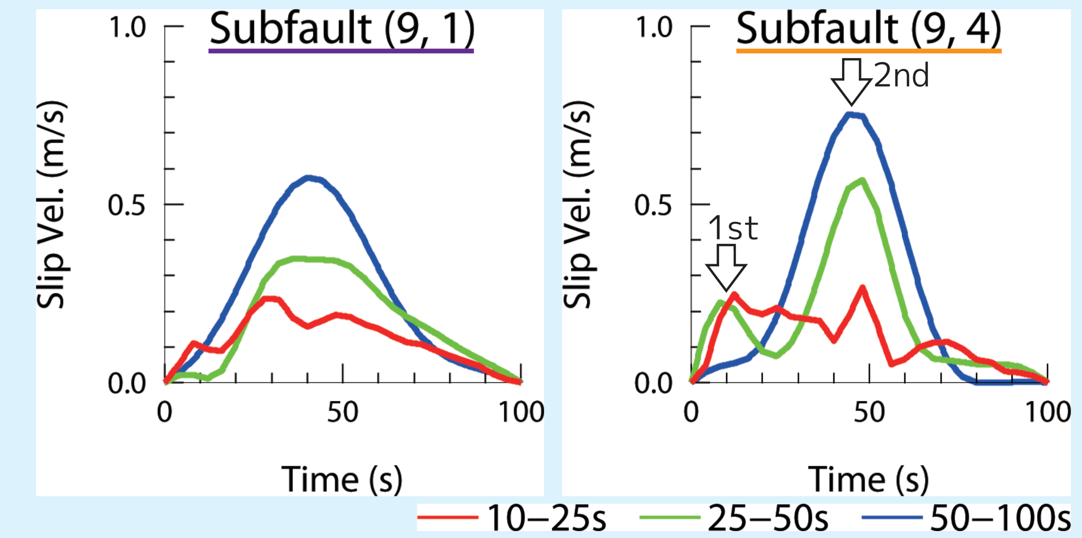

Source Image & Discussion

The source image for the 2011 Tohoku earthquake on the period band of 10-100s is summarized as follows:

① (1st) Deep rupture off Miyagi rupture at 0-60s toward down-dip radiating relative short period (10-25s) seismic waves.
② Shallow rupture off Miyagi at 45-90s toward up-dip with long duration and huge slip radiating long period seismic wave.
③ (2nd) Deep rupture off Miyagi rupture at 45-90s toward down-dip radiating long period (25-100s) seismic waves.
④ Deep rupture off Fukushima at 90-150s.

* Some differences between the source models estimated by teleseismic and strong-motion data are probably because of the limitations unique to each dataset. The examination on the limitations and the construction of source image keeping its result in mind will be a next step of our study.

■ Source image for the 2011 Tohoku earthquake

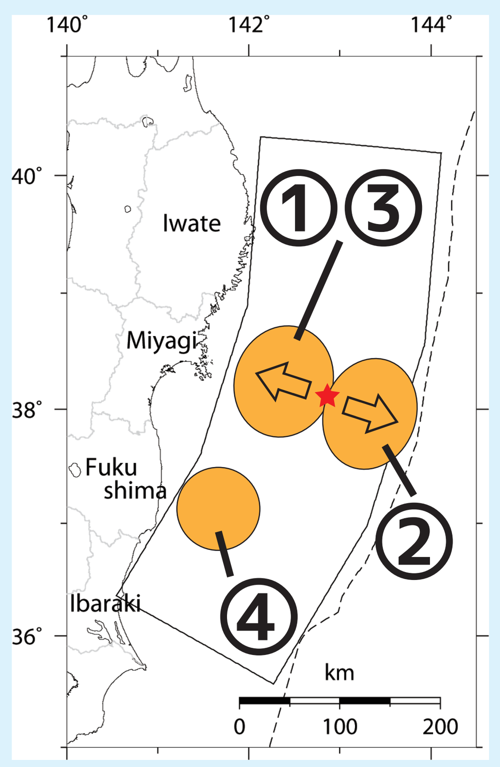

■ Large earthquake distribution

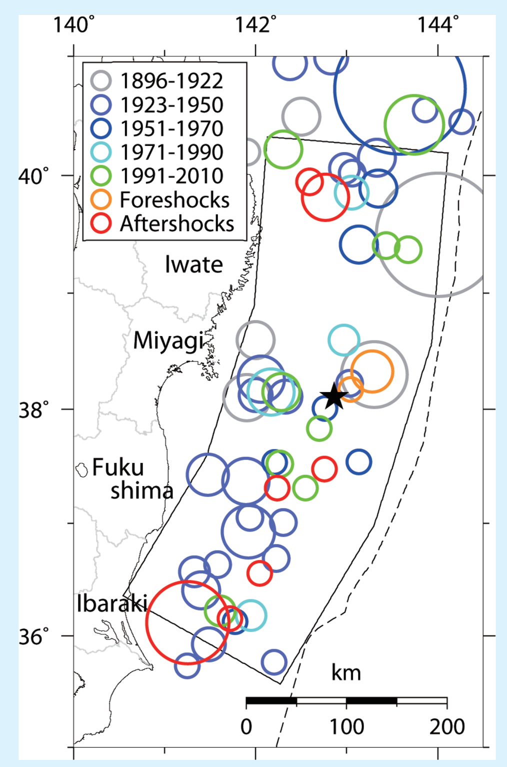

* Open circles denote the source areas of the large interplate earthquakes (M≧6.8) from 1896 to 2012, which were selected from Usami et al. (2013) and the JMA catalog.

■ P-wave tomographic image

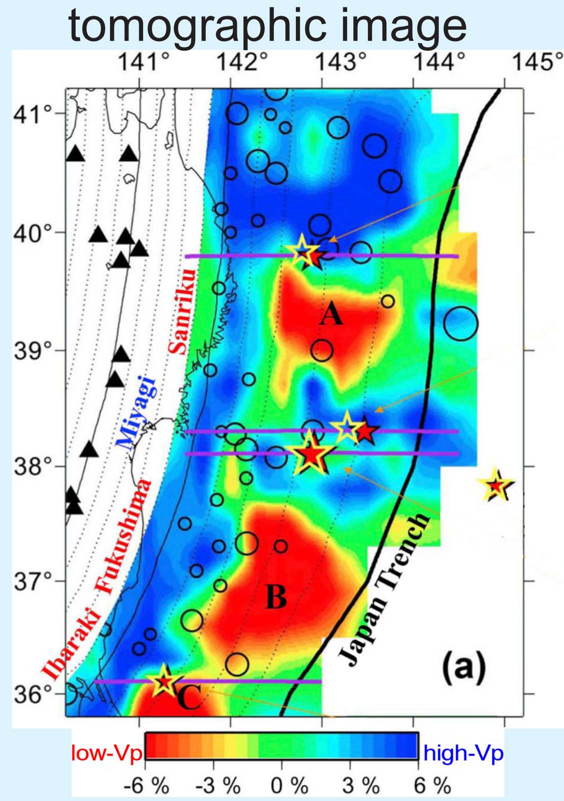

* Modified figure from Zhao et al. (2011). This describes the Vp image above the upper boundary of the subducting Pacific slab.

・Overlap between the deep ruptures (①③④) and the past interplate earthquakes
→ Reactivation for the pre-existing asperities of the past earthquakes

・Comparison with the seismic tomographic image on the plate boundary off Tohoku area (e.g., Zhao et al., 2011) shows that the rupture zones (①②③④) overlap with not the low-velocity (red) zone but the high-velocity (blue) zone.
→ Rupture process controlled by structural heterogeneities on the plate boundary

・Depth variation of fault rupture off Miyagi (①③ vs ②) may be explained by geometries of the subducting plate (e.g., Ito et al., 2005) or geological structural changes (e.g., Miura et al., 2005)

・**The dominant-period difference in the seismic-wave radiation between ① and ③ may result from the mechanism that the second rupture is smoother than the first one because small-scale heterogeneities on the fault are removed by the first one.**

■ Schematic illustration of the geological structure off Miyagi

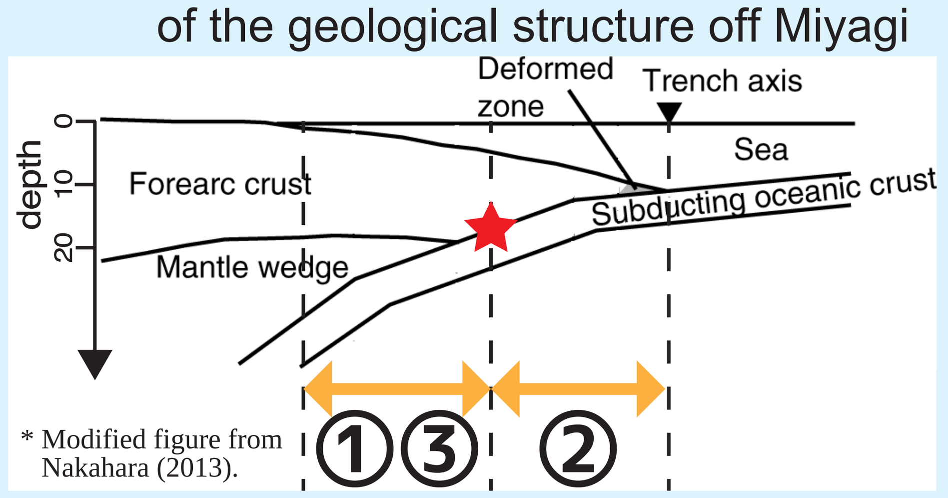

* Modified figure from Nakahara (2013).

■ Data fitting examples

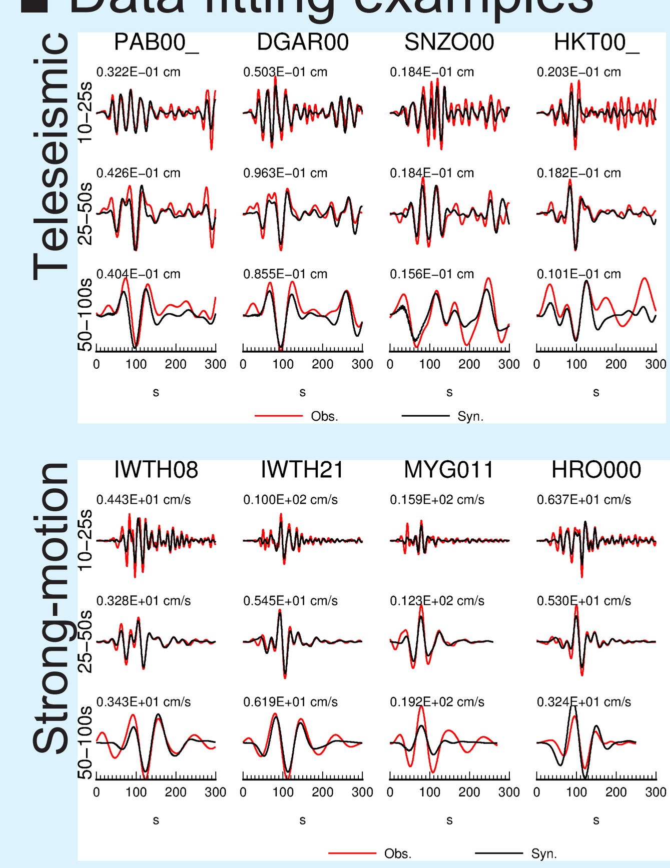

References:
Asano and Iwata (2012), Earth Planets Space, 64, 1111-1123.
Aoi & Fujiwara, (1999), Bull. Seismol. Soc. Am., 89, 918-930.
Efron, B. (1982), Society for Industrial and Applied Mathematics,92 pp.
Hartzell & Heaton, (1983), Bull. Seismol. Soc. Am., 73, 1553-1583.
Ide et al., 2011, Science, 332, 1426–1429.
Ito et al., (2005), Geophys. Res. Lett., 32, L05310.
Koketsu et al., (2012), 15th WCCE, No.1773.
Koper et al., (2011), Earth Planets Space, 63, 599–602.
Kubo & Kakehi, (2013), Bull. Seismol. Soc. Am., 103, 1195-1220.
Miura et al., (2005), Tectonophysics, 407, 165–188.
Nakahara, (2013), Bull. Seismol. Soc. Am., 103, 1348-1359.
Usami et al., (2013), University of Tokyo Press, 693 pp.
Zhao et al., (2011), Geophys. Res. Lett., 38, L17308.

Acknowledgement:
The teleseismic waveform data supplied by IRIS - DMC, the strong-motion data recorded by K-NET, KiK-net, and F-net of NIED, and the JMA unified hypocenter catalog were used for the analysis.